INSTITUTE OF PHYSICS PUBLISHING PHYSICS IN MEDICINE AND BIOLOGY

Phys. Med. Biol. **51** (2006) 6005–6021 doi:10.1088/0031-9155/51/23/004

A technique to consider mismatches between fMRI and EEG/MEG sources for fMRI-constrained EEG/MEG source imaging: a preliminary simulation study

Chang-Hwan Im[1] **and Soo Yeol Lee**[2]

[1] Department of Biomedical Engineering, Yonsei University, 234 Maejiri, Heungeop-myun, Wonju-si, Kangwon-do, 220-710, Korea
[2] Department of Biomedical Engineering, Kyung Hee University, Yongin, 446-701, Korea

E-mail: ich@yonsei.ac.kr

Received 17 July 2006, in final form 22 August 2006
Published 30 October 2006
Online at stacks.iop.org/PMB/51/6005

Abstract

fMRI-constrained EEG/MEG source imaging can be a powerful tool in studying human brain functions with enhanced spatial and temporal resolutions. Recent studies on the combination of fMRI and EEG/MEG have suggested that fMRI prior information could be readily implemented by simply imposing different weighting factors to cortical sources overlapping with the fMRI activations. It has been also reported, however, that such a hard constraint may cause severe distortions or elimination of meaningful EEG/MEG sources when there are distinct mismatches between the fMRI activations and the EEG/MEG sources. If one wants to obtain the actual EEG/MEG source locations and uses the fMRI prior information as just an auxiliary tool to enhance focality of the distributed EEG/MEG sources, it is reasonable to weaken the strength of fMRI constraint when severe mismatches between fMRI and EEG/MEG sources are observed. The present study suggests an efficient technique to automatically adjust the strength of fMRI constraint according to the mismatch level. The use of the proposed technique rarely affects the results of conventional fMRI-constrained EEG/MEG source imaging if no major mismatch between the two modalities is detected; while the new results become similar to those of typical EEG/MEG source imaging without fMRI constraint if the mismatch level is significant. A preliminary simulation study using realistic EEG signals demonstrated that the proposed technique can be a promising tool to selectively apply fMRI prior information to EEG/MEG source imaging.

(Some figures in this article are in colour only in the electronic version)

1. Introduction

Current haemodynamic measurements, particularly functional magnetic resonance imaging (fMRI), can provide excellent spatial resolution as high as 1 mm, but are temporally limited from several seconds to several minutes. In contrast, EEG and MEG have superior temporal resolutions compared to fMRI, which allow studies of the dynamics of neural networks that occur on the order of tens of milliseconds. Unfortunately, the spatial resolution of EEG and MEG does not match that of fMRI due to their limited numbers of spatial measurements and ambiguity of electromagnetic inverse problems (Dale *et al* 2000). Therefore, effective combinations of the two different kinds of modalities might provide new insight that could not be achieved with either modality alone.

The approaches for combining fMRI results with EEG/MEG measurements can be classified into two major categories: one is the equivalent current dipole (ECD) model and the other is the distributed source model, which is sometimes called EEG/MEG cortical source imaging.

The ECD model is the most common and straightforward approach to the multimodal data fusion. The most widely used model is to assume a relatively small number of rotating dipole sources, of which the initial positions are placed in fMRI activation foci (Ahlfors *et al* 1999, Korvenoja *et al* 1999, 2001). The locations of the current dipoles are then adjusted using nonlinear fitting algorithms such as the Levenberg–Marquardt algorithm (LMA), Nelder–Meade downhill simplex searches and so on. The orientations and strengths of the ECDs are determined using a least-squares algorithm. Wagner *et al* (2000) constrained the dipoles to stay within a maximum distance from their seed points. A penalty term was added to the error function if the distance from their seed points exceeded a predetermined maximum distance. Orpitz *et al* (1999), Torquati *et al* (2005) and Vanni *et al* (2004) constrained the dipole locations and/or orientations based on the anatomical and functional priors, and then estimated temporal changes of the dipoles. These simple combinations of multimodal data can solve conventional problems of the ECD model that the number and initial locations of the ECDs cannot be estimated *a priori*. However, these approaches still have a potential problem. When applying the ECD model, we should consider the effect of 'crosstalk', which represents the influence of other dipoles to a dipole nearest to an actual source (Liu *et al* 1998, Fujimaki *et al* 2002). From their simulation studies, it was observed that constraining multiple dipole sources in all the possible fMRI activation foci might yield considerable error if some of the ECD locations were not correctly estimated.

Contrary to the ECD model, the distributed source model or EEG/MEG source imaging assumes a lot of current dipoles scattered in source spaces and the orientations and/or strengths of the dipoles are determined using linear (L2 norm) or nonlinear (L1 norm) estimation methods. Based on the basic idea, Dale and Sereno (1993) first proposed constraining the source space into anatomically known locations (interface between white and grey matter of the cerebral cortex extracted from MRI) and orientations (perpendicular to the cortical surface), and weighting the estimate based on *a priori* information. In the paper, they first addressed the possibility of the fMRI-guided EEG/MEG distributed source solutions. The distributed source approaches can be readily incorporated with fMRI data and are more biologically plausible than the ECD model since it uses anatomical prior information. The most straightforward way to impose the fMRI constraint upon the distributed source reconstruction is to restrict the source spaces to locations exceeding a threshold predetermined for fMRI statistical analyses (George *et al* 1995), which is still being frequently used (Phillips *et al* 2005). According to Liu *et al*'s (1998) study, however, this approach is very sensitive to some generators of EEG or MEG signals that are not detected by fMRI, which have been usually referred to as 'fMRI

invisible sources'. Liu *et al* (1998) revealed that the distortion by the fMRI invisible sources could be reduced considerably by just giving a constant weighting factor to the diagonal terms of source covariance matrix in a linear inverse operator. They also suggested that the optimal fMRI weighting for the non-activation regions should be 10% of the maximum value, in order to minimize the distortion due to both fMRI invisible and visible sources. Some research groups have been using different weighting methods and values, e.g. Wagner *et al* (2000, 2001) and Babiloni *et al* (2003, 2004), but their basic concepts remained the same as that of Liu *et al*'s approach in that they also gave different weighting factors to sources inside and outside the fMRI active areas. Recently, Bayesian approaches have been successfully applied to the multimodal imaging (Sato *et al* 2004, Phillips *et al* 2005) and demonstrated that the approaches can reduce the influence of fMRI extra sources compared to the conventional Wiener estimation approaches.

Using such an fMRI-constrained EEG/MEG source imaging technique, one could obtain spatially more focalized EEG/MEG source distribution with a reduced number of spurious sources as well as observe dynamic temporal changes of static fMRI sources (Liu *et al* 1998, 2002, Bonmassar *et al* 2001, Dale *et al* 2000, Lin *et al* 2004).

The fMRI-constrained distributed source reconstruction showed powerful advantages in such applications when fMRI and EEG/MEG sources are corresponding well with each other. In many practical cases, however, there sometimes exist significant mismatches between fMRI and EEG/MEG sources. Vitacco *et al* (2002) investigated the difference between fMRI and EEG/MEG sources using a semantic monitoring task. To deal with the different spatiotemporal resolutions of the two modalities, they averaged their LORETA (low resolution electromagnetic tomography) (Pascual-Marqui *et al* 1994) values across all temporal epochs, and attempted to identify each LORETA local maximum with its nearest fMRI local maximum in a statistically meaningful manner. They found that this could be done for group mean data, but on an individual basis only half of the subjects showed significant correspondence between the fMRI and LORETA patterns. These mismatches are bound to occur due to the limited spatial sensitivity pattern of EEG/MEG sensors and the limited time resolution of fMRI (Gonzalez Andino *et al* 2001, Ahlfors and Simpson 2004). Some source activity may be located or oriented such that there is little electromagnetic field outside the head. Examples of this are radially oriented sources in MEG and deep 'closed field' sources in EEG, for which the activity patterns are such that the total macroscopic current cancels out. All of these could generate significant fMRI but not in EEG or MEG. Furthermore, the fMRI activations can be detected where there are no neuronal activities because the fMRI signal is sensitive to parameters reflecting energy consumption. In practice, the brain consumes energy for many more processes which are not directly linked to the neuronal activities, e.g. neurotransmitter release and uptake, vesicular recycling, maintenance of membrane potentials and so on (Rothman *et al* 1999). These kinds of sources are usually referred to as 'fMRI extra sources', which have been generally ignored in many studies due to their little effect on the fMRI-constrained source estimates (e.g., Ahlfors and Simpson (2004)). On the other hand, some EEG/MEG sources cannot be detected in fMRI, which have been usually referred to as 'fMRI invisible sources'. Some neuronal sources which are active only for a short time period may be detected in EEG or MEG, but do not appear in fMRI results since fMRI integrates brain activity over time. Another type of mismatch is originated from an intrinsic discrepancy between fMRI and EEG/MEG due to the fundamental difference of haemodynamic and electrophysiological processes (Disbrow *et al* 2000, Nunez and Silberstein 2000, Bonmassar *et al* 2001), which can be called 'fMRI displacement sources'.

If no fMRI mismatch sources exist, i.e. the fMRI activation regions can cover all EEG/MEG generators, the EEG/MEG source distribution can be focalized by using the

fMRI constraint. Moreover, the use of the fMRI prior information can reduce spurious or phantom sources generated due to the *ill-posedness* of EEG/MEG inverse problems. On the other hand, the EEG/MEG can provide temporal information for the static fMRI results. However, it has been frequently reported that the fMRI activation regions are still sensitive to the existence of some significant fMRI invisible sources or mismatch sources when the conventional weighting approaches are applied (Fujimaki *et al* 2002, Ahlfors and Simpson 2004, Im *et al* 2005), and such mismatches may cause severe distortions or elimination of meaningful EEG/MEG sources (Ahlfors and Simpson 2004, Im *et al* 2005, Liu *et al* 2006).

Therefore, if one tries to identify the actual EEG/MEG source locations and uses the fMRI prior information as just an auxiliary tool to enhance focality of the distributed EEG/MEG sources, it can be a smarter choice to weaken the strength of fMRI constraint or even not to use the fMRI constraint at all when severe mismatches between fMRI and EEG sources are observed (Vitacco *et al* 2002, Gonzalez Andino *et al* 2001).

In the present paper, we have proposed an alternative technique to automatically adjust the strength of fMRI constraint considering the mismatch level. We controlled the weakness of the fMRI constraint by adjusting the prior activation regions, not by changing the weight values, since no absolutely satisfactory weighting values which can perfectly recover the missing or distorted source distributions can be found (Im *et al* 2005). When there are significant EEG/MEG sources lying outside fMRI activation regions, the prior regions are automatically expanding to include the missing EEG/MEG sources into the prior activation regions. Although some loss of the focality in the resultant EEG/MEG source images is inevitable, we can estimate more plausible EEG/MEG source locations instead. The use of the proposed technique rarely affects the results of fMRI-constrained EEG/MEG source imaging if no major mismatch between the two modalities is detected; while the new results become similar to those of conventional EEG/MEG source imaging without fMRI constraint, if the mismatch level is significant. In the present study, we demonstrated the feasibility of the proposed technique using artificially constructed EEG data, assuming different mismatch levels. Since the inverse algorithms used for the EEG source imaging are identical to those for the MEG source imaging, the proposed technique can also be applied to MEG studies without any modifications.

2. Methods

2.1. Forward calculation and inverse estimation

In the present study, a realistic geometry head model was used for accurate EEG forward calculation (He *et al* 1987, Hämäläinen and Sarvas 1989). A first-order node-based boundary element method (BEM) was applied to construct a lead field matrix which relates source locations to scalp electrodes. In the present study, three-layer tessellated boundary surfaces, consisting of inner and outer skull boundaries and scalp surface, were generated using CURRY5 for windows (Compumedics, Inc., El Paso, TX, USA) from structural MRI data. The boundary element models consisted of 5372 boundary elements and 2748 surface nodes. For all realistic simulations performed in the present study, the MNI standard brain atlas (http://www.mrc-cbu.cam.ac.uk/Imaging/Common/mnispace.shtml#evans_proc) was utilized. The relative conductivity values of brain, skull and scalp were assumed to be 1, 1/16 and 1, respectively (Haueisen *et al* 1997, Oostendorp *et al* 2000).

Since synchronously activated pyramidal cortical neurons, which are located perpendicularly on the cortical surface, are widely believed to be the main EEG and MEG generators, many recent studies have adopted this physiological phenomenon as a basic

anatomical constraint in EEG or MEG source imaging (Dale and Sereno 1993, Kincses *et al* 1999, Dale *et al* 2000, Babiloni *et al* 2003). The source imaging with such an anatomical constraint, which has often been called the cortically distributed source model or cortical source imaging, resulted in elimination of spurious sources (Baillet *et al* 2001) as well as reduction of crosstalk distribution (Liu *et al* 1998), compared to conventional volume-based imaging techniques.

To impose the anatomical constraint, many dipolar sources are placed on the cortical surface extracted and tessellated from structural MRI data. Although developments of medical image processing and high resolution structural MRI enabled us to get high resolution cortical surface with sub-millimetre modelling errors (Dale *et al* 1999, Fischl and Dale 2000), it is computationally inefficient to use whole cortical surface vertices for the source reconstruction purpose because of the increased underdetermined relationship between limited numbers of sensors and larger numbers of source locations. To reduce the number of possible source locations, a smaller number of vertices was downsampled from the cortical surface as regularly as possible and used for source reconstruction purposes; whereas the original mesh information was used only for visualization purposes (Dhond *et al* 2003, Lin *et al* 2004). In the present study, about 15,000 vertices were downsampled from more than 400,000 original cortical vertices.

To reconstruct the cortically distributed brain sources, we used a linear estimation approach (Dale and Sereno 1993, Dale *et al* 2000). The expression for the inverse operator **W** is

$$\mathbf{W} = \mathbf{R}\mathbf{A}^{\mathrm{T}}(\mathbf{A}\mathbf{R}\mathbf{A}^{\mathrm{T}} + \lambda^2\,\mathbf{C})^{-1}, \tag{1}$$

where **A** is a lead field matrix, **R** is a source covariance matrix and **C** is a noise covariance matrix. The source distribution can be estimated by multiplying the measured signal at a specific instant x by **W**. If we assume that both **R** and **C** are scalar multiples of identity matrix, this approach becomes identical to minimum norm estimation (Liu *et al* 2002). In this study, the source covariance matrix **R** was assumed to be a diagonal matrix, which means that we ignored relationships between neighbouring sources. The minimum norm estimation is known to have a bias towards superficial currents, caused by the attenuation of the lead fields with increasing source depth. It is possible to compensate for this tendency by scaling the columns of **A** with a function increasing monotonically with the source depth (Gorodnistky *et al* 1995, Lin *et al* 2004). Each entry in the kth column of **A** was normalized by dividing it by $\left(\mathbf{a}_k^{\mathrm{T}}\mathbf{a}_k\right)^{1/2}$, where $\mathbf{a}_k$ is a kth column vector of the lead field matrix **A**. In this study, a pre-stimulus time window was used to calculate **C**. λ^2 is a regularization parameter and was determined using the L-curve method (Hansen 1992).

We imposed the fMRI constraint by giving different weighting values to the diagonal terms of **R**. Without considering fMRI priors, **R** is an identity matrix. When imposing fMRI constraints, the diagonal terms of **R** were set to 1 for source locations within fMRI activation regions; while they were set to 0.1 for source locations outside fMRI activation regions (Liu *et al* 1998, 2002) in order to minimize distortion of source patterns stemming from both fMRI visible and invisible sources (Liu *et al* 1998).

2.2. Automatic expansion of prior activation regions

As briefly explained before, fMRI-constrained EEG/MEG source imaging might result in false EEG/MEG source estimates when the fMRI activation regions do not cover actual EEG/MEG source locations. Figure 1 shows a schematic diagram to elucidate the influence of the false fMRI information, where actual neuronal source locations are presented as vertical arrows.

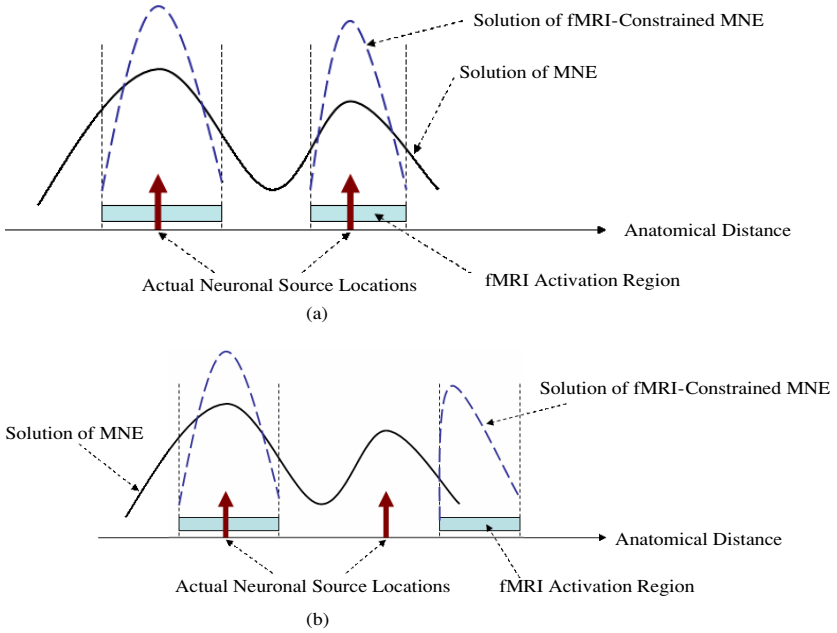

Figure 1. Schematic diagrams to elucidate the influence of mismatch sources upon the estimated source images: (a) fMRI activation regions cover two actual source locations; (b) fMRI activation regions do not cover one of the neuronal source locations. Solutions of fMRI-constrained source imaging might be distorted when fMRI activation region cannot cover actual neuronal source locations.

As presented in figure 1(a), the fMRI-constrained inverse solution tends to be more focalized than the conventional linear inverse solution when fMRI activation regions cover the actual source locations. As seen in figure 1(b), however, fMRI-constrained source imaging generally yields distorted or false source estimates when there are mismatches between fMRI prior activation regions and actual neuronal source locations. Such phenomena will be demonstrated again through our simulation study which will be presented later.

Although one of the important aims of the fMRI-constrained EEG/MEG source imaging is obtaining more focalized EEG/MEG source distribution and reducing spurious or phantom sources which stem from *ill-posed* characteristic of EEG/MEG inverse problems, accurate estimation of actual neuronal sources should not be underestimated. Thus, the authors suggest that the missing source locations should be included in the prior activation regions when there are severe mismatches between the two modalities. To implement such an idea, a criterion was introduced to quantitatively assess the mismatches between the fMRI activation regions and the EEG/MEG source locations.

We first reconstructed distributed EEG/MEG sources at every time slice without fMRI *a priori* information and integrated the source intensities over the whole time window considered. Since the integration over the whole time window might lose some significant signal generators of which the durations are relatively short, we used a 'partial integration' defined as follows:

$$J_i = \max\left\{\int_0^{\Delta t} j_i(t)\,\mathrm{d}t, \int_{\Delta t}^{2\Delta t} j_i(t)\,\mathrm{d}t, \ldots, \int_{(n-1)\Delta t}^{n\Delta t} j_i(t)\,\mathrm{d}t\right\}, \tag{2}$$

where J_i is the partially integrated source intensity at ith cortical vertex, $j_i(t)$ is the source intensity at a time slice t and Δt is the time interval when the whole time window is divided into n sub-windows. In our simulation studies, Δt was set as 30 ms when sampling rate was 500 Hz. After the process, we can have the information on the locations of possible significant sources.

We then calculated an average of the partially integrated source intensities, Q_{AVE}, for all cortical vertices which belong to the fMRI activation regions. The averaged value was used for setting a threshold which was used when including source points outside the fMRI activation regions into the new prior activation regions. The threshold was defined as

$$\mathrm{Thres} = Q_{\mathrm{AVE}} \times p, \tag{3}$$

where p is a user-defined scalar of which the range is between 0 and $Q_{\mathrm{MAX}}/Q_{\mathrm{AVE}}$, when Q_{MAX} is the maximum value among the partially integrated source intensities. Then, the source points outside the fMRI activation regions, of which the integrated source intensities exceed Thres, were included in the new prior activation regions, while maintaining the original fMRI activation regions. If one selects 0 as the p value, the prior activation regions will cover the whole source space, resulting in normal linear inverse solutions without fMRI constraint. In contrast, if a p value of $Q_{\mathrm{MAX}}/Q_{\mathrm{AVE}}$ is selected, the prior activation regions will remain unchanged because Thres equals Q_{MAX}. The introduction of this user-defined scalar can allow the users to decide the strength of the proposed technique when the technique is implemented in a general software package. The selection of large p values results in highly constrained source images; whereas that of small p values results in widespread source distributions similar to conventional linear inverse solutions without *a priori* information. In the present simulation study, we set the p value as 1, which means that we used Q_{AVE} as the threshold value.

Figure 2 shows schematic diagrams to elucidate the proposed technique. When the proposed technique is applied to an example in figure 1(a), where the fMRI activation regions cover all actual neuronal sources, the extension of the prior activation regions is not considerable because no significant activations exceeding Q_{AVE} are found outside the fMRI activation regions (see figure 2(a)). Then, the resultant fMRI-constrained EEG/MEG source estimates will not be much different from the conventional fMRI-constrained source estimates. On the other hand, when the proposed technique is applied to an example shown in figure 1(b), where one significant missing source exists outside the fMRI activation regions, the regions around the missing source location are included in the new prior activation regions since the EEG or MEG source estimates around the neuronal source are significant enough to exceed the threshold value (see figure 2(b)). In such a case, the value of Q_{AVE} becomes smaller than that of the previous case because there is no significant EEG/MEG source inside one of the fMRI activation regions, which results in unnecessarily large extension of the prior activation regions. Thus, the use of the proposed technique may lose the focality of the source estimate which is one of the main advantages of fMRI-constrained EEG/MEG source imaging. Instead of sacrificing the focalized source distribution, however, one can estimate more accurate source locations. Therefore, the proposed technique can be a promising tool allowing 'selective' application of fMRI prior information to EEG/MEG source imaging.

2.3. Simulation set-ups

Neuroelectromagnetic inverse problems (NIP) are hard to verify by *in vivo* experiments because exact source locations inside the real human brain cannot be estimated *a priori*. For that reason, artificially constructed forward data are widely used to validate EEG and MEG inverse algorithms (Kincses *et al* 1999, Sekihara *et al* 2001). Hence, in the present simulation study, we applied the proposed approach to artificially constructed EEG data.

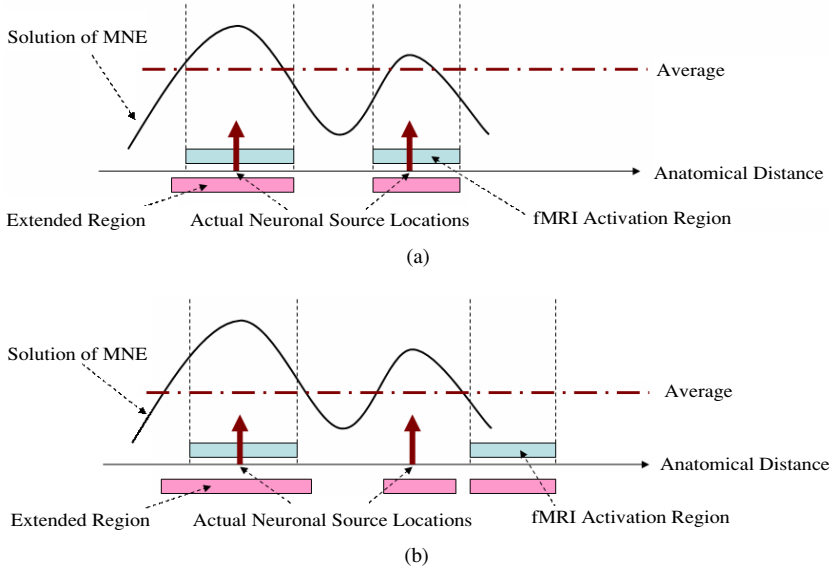

Figure 2. Schematic diagrams to elucidate the concept of the proposed technique: (a) when the fMRI activation regions cover all the actual neuronal sources, the extension of the prior activation regions is not considerable because no significant activations exceeding Q_{AVE} are found outside the fMRI activation regions; (b) when one significant missing source exists outside the fMRI activation regions, the neuronal source location is included in the new prior activation regions since the EEG or MEG source estimates around the neuronal source are significant enough to exceed the threshold value.

We adopted realistic conditions to construct the artificial EEG data. We assumed that 128 electrodes were attached to a subject's scalp according to the extended 10–20 electrode system. To utilize anatomical information, interface between white and grey matter was extracted from MRI T1 images of an MNI standard brain and tessellated into 865 712 triangular elements and 432 654 vertices. To extract and tessellate the cortical surface, we applied *BrainSuite* developed in the University of Southern California, CA, USA (Shattuck and Leahy 2002). For the accurate forward calculation, full head structures were taken into account and BEM was applied.

Nowadays, for the forward simulations, generating artificial activation patches on a brain cortical surface has been popularized instead of activating some point sources (Im *et al* 2003). To generate the activation patches and construct a forward data set, a concept named virtual area was adopted. An activation patch was generated using the following process: (1) a point is selected as a seed of an activation patch area. (2) The patch area is extended by including neighbouring vertices around the patch. (3) If the total virtual area of the cortical patch exceeds an aimed surface area, the extension of the activation patch is terminated.

3. Simulations and results

For the present simulation study, we assumed three cortical patches as shown in figure 3, where source 3 is hidden inside the Sylvain fissure of right hemisphere. The cortical activation patches were made of sets of dipoles with constant current density and orientations perpendicular to the cortical surface. Then, the current dipole moment at each vertex was calculated by the

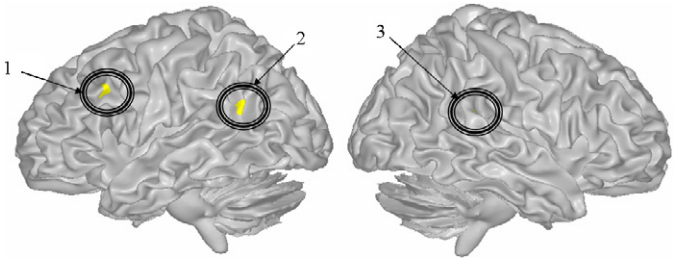

Figure 3. Locations of three cortical patches assumed to simulate a realistic EEG signal.

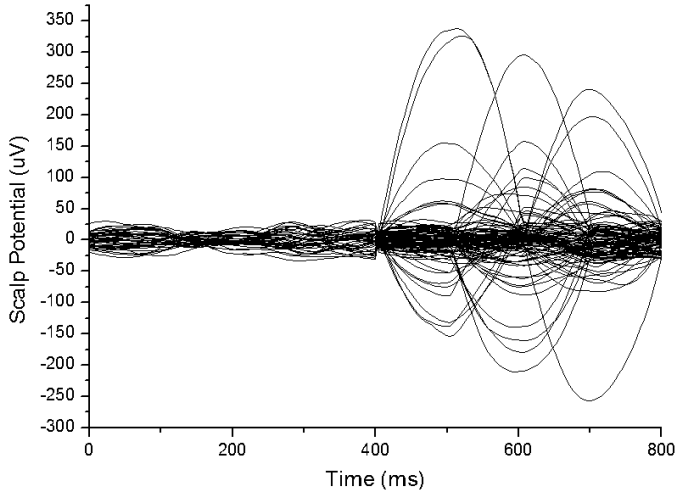

Figure 4. Simulated EEG signals with real background EEG signal (SNR = 7 dB).

product of the current density and the virtual area. The temporal variations of current density of the three source patches were assumed as follows:

Source 1

$$J = -0.6 \times 10^{-4}(t - 500)^2 + 0.6 \quad (400\ \text{ms} \leqslant t < 600\ \text{ms})$$
$$= 0 \quad (0\,\text{ms} \leqslant t < 400\ \text{ms}, 600\ \text{ms} \leqslant t < 800\ \text{ms})$$

Source 2

$$J = -0.6 \times 10^{-4}(t - 600)^2 + 0.6 \quad (500\ \text{ms} \leqslant t < 700\ \text{ms})$$
$$= 0 \quad (0\,\text{ms} \leqslant t < 500\ \text{ms}, 700\ \text{ms} \leqslant t < 800\ \text{ms})$$

Source 3

$$J = -0.6 \times 10^{-4}(t - 700)^2 + 0.6 \quad (600\ \text{ms} \leqslant t < 800\ \text{ms})$$
$$= 0 \quad (0\,\text{ms} \leqslant t < 600\ \text{ms}).$$

After calculating electric potentials at the 128-channel electrodes assuming a 500 Hz sampling rate, we added real background EEG signals, which were obtained from a pre-stimulus period of a practical EEG experiment. The original signal without noise was scaled in order for the signal-to-noise ratio (SNR) to be approximately 7 dB. Figure 4 shows the artificial EEG signals with respect to time.

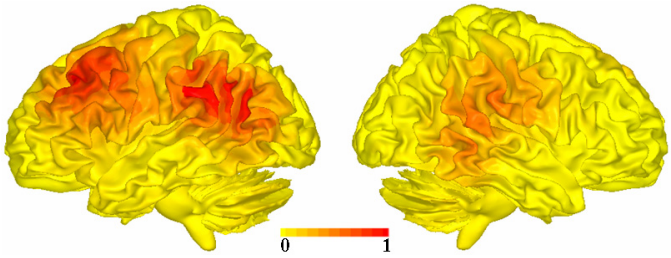

Figure 5. Possible significant source map obtained from partial time integration of conventional source estimates. The values were normalized to maximum.

To apply the proposed technique to the simulated EEG signals, we first reconstructed source images using the conventional linear inverse operator without fMRI constraint at every time slice (from 0 ms to 800 ms). The time-varying source intensity at every cortical vertex was then partially integrated using (2), resulting in the possible significant source map shown in figure 5. We can see from the figure that the partially integrated source distribution correctly represents rough locations of the presumed cortical sources. Then, four different cases of fMRI activation regions, of which the areas were nearly identical, were assumed as follows:

Case 1. All fMRI activation regions cover the actual EEG source locations (perfectly matching)—figure 6(a).
Case 2. Two fMRI activation regions cover actual EEG source locations (sources 1 and 2), but the other does not cover source 3—figure 6(b).
Case 3. One fMRI activation region covers the location of source 1, but the other two regions do not cover the actual source locations (sources 2 and 3)—figure 6(c).
Case 4. No fMRI activation regions cover the actual EEG source locations—figure 6(d).

For each case considered, we applied the proposed technique and generated new prior activation regions. Figure 7 shows the comparison between original and modified prior activation regions. It can be seen from the figures that the prior activation regions were extended to include the EEG source locations, when there are significant mismatches between fMRI prior activation regions and actual EEG sources.

We then compared the source distributions reconstructed at three time slices—500 ms, 600 ms and 700 ms, under three different conditions: (1) no fMRI constraint, (2) with original prior activation regions and (3) with modified prior activation regions. Figure 8 shows the reconstructed source distributions for case 1, where normalized current dipole power (sum of squared dipole component strengths) was used for visualization purposes and noisy sources of which the normalized power is below 0.1 were excluded in the visualization. The following facts could be observed from the results: (1) more concentrated source distributions could be estimated by using the fMRI prior information as a functional constraint; (2) when the fMRI prior activation regions cover all the actual source locations, the source distributions estimated with modified prior activation regions were similar to those estimated with original prior activation regions.

Figures 9 and 10 show the source distributions reconstructed for case 2 and case 3, respectively, when one or two EEG sources are mismatched with the original prior activation regions. As seen from the source estimates, the use of false fMRI information can yield severe distortion or misidentification of EEG source distributions. In contrast, the use of

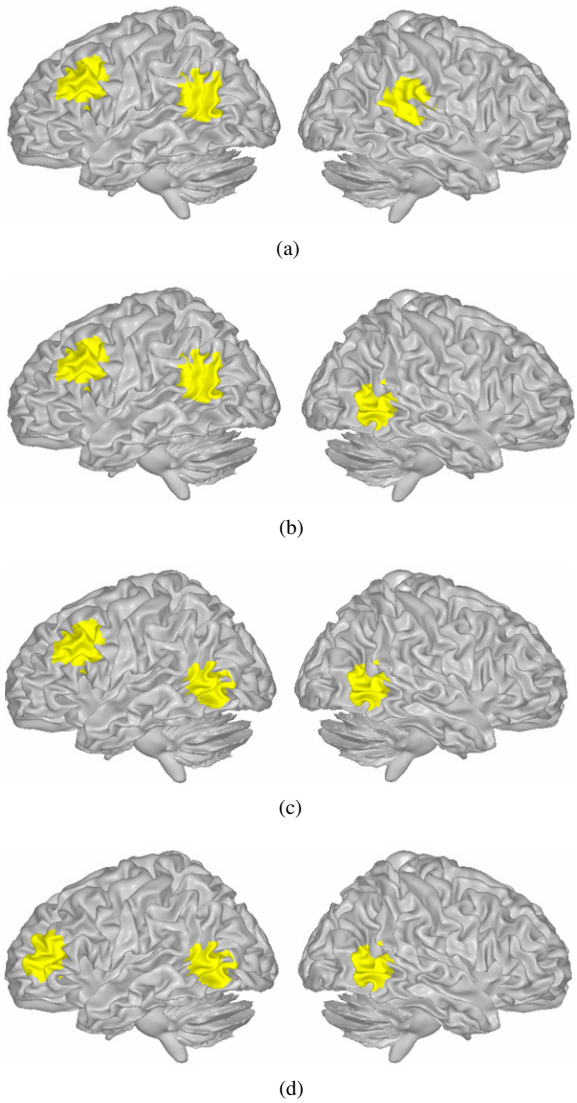

Figure 6. Four different cases of fMRI activation regions: (a) case 1—no mismatch source; (b) case 2—one mismatch source; (c) case 3—two mismatch sources; (d) case 4—three mismatch sources. Compare the fMRI activation locations with actual source locations in figure 4.

modified prior regions resulted in more widespread source images compared to the original fMRI-constrained source images, but we could identify the actual source locations more appropriately. It was also observed that the more mismatched sources yielded the wider source distribution. Nevertheless, it is obvious that widespread but reasonable source distribution is still more useful than the inaccurate source identification with focal distribution in many practical applications.

Figure 11 shows the reconstructed source distributions for case 4, when all fMRI prior regions do not coincide with the actual EEG source locations. All the sources were not correctly estimated when the original prior activation regions were used; whereas the source distribution

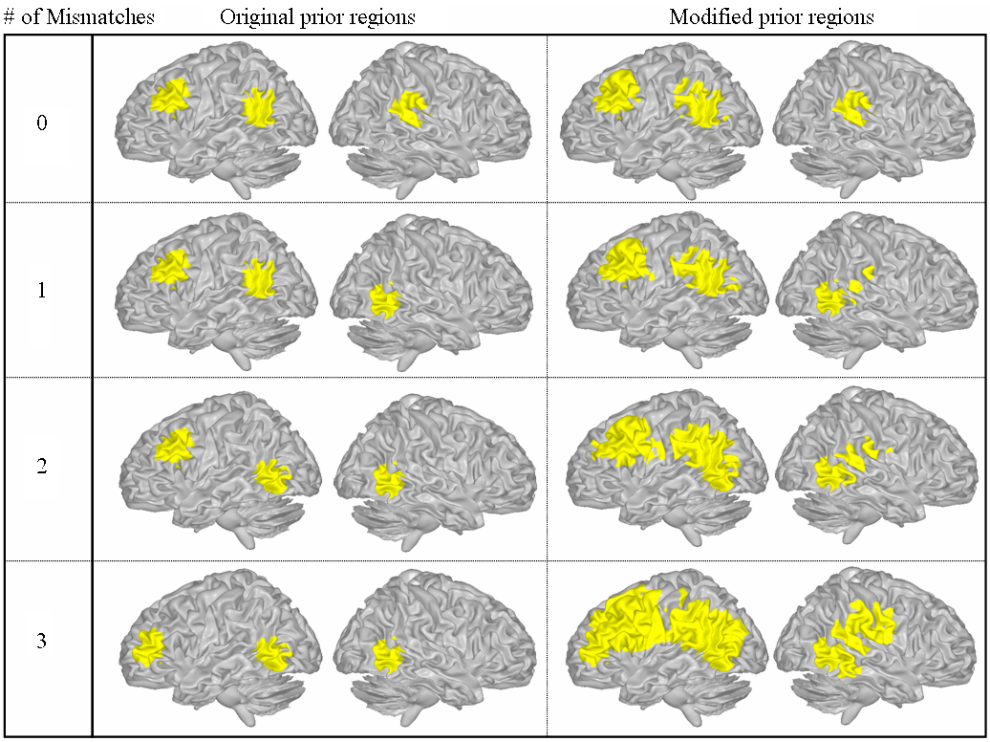

Figure 7. Comparison between original prior regions and modified prior regions. The numbers in the first column represent the number of mismatch sources. Cortical surfaces shown in second and third columns represent original and modified prior regions, respectively.

Table 1. Mean localization errors (mm) of the estimated current density maps. The values are averaged errors of three source estimates at 500 ms, 600 ms and 700 ms. The mean error of the 'no fMRI prior' case was 9.72 mm.

Cases	Original prior	Modified prior
Case 1	8.05	8.24
Case 2	13.04	9.17
Case 3	17.33	9.46
Case 4	22.78	9.79

estimated with modified prior activation regions yielded source distributions similar to the linear inverse solutions estimated without fMRI prior information, which means that one should not expect the advantage of fMRI-constrained EEG source imaging any more when there are significant mismatches between fMRI and EEG sources. In practice, however, priority should be given to estimating accurate EEG source locations, as explained before.

Table 1 shows the localization error (distance between presumed source location and peak position of current density estimates) averaged for three time slices. The localization error increased as the mismatch became severe when original prior activation regions were used; whereas the error was not influenced much by the mismatch level when modified prior activation regions were used.

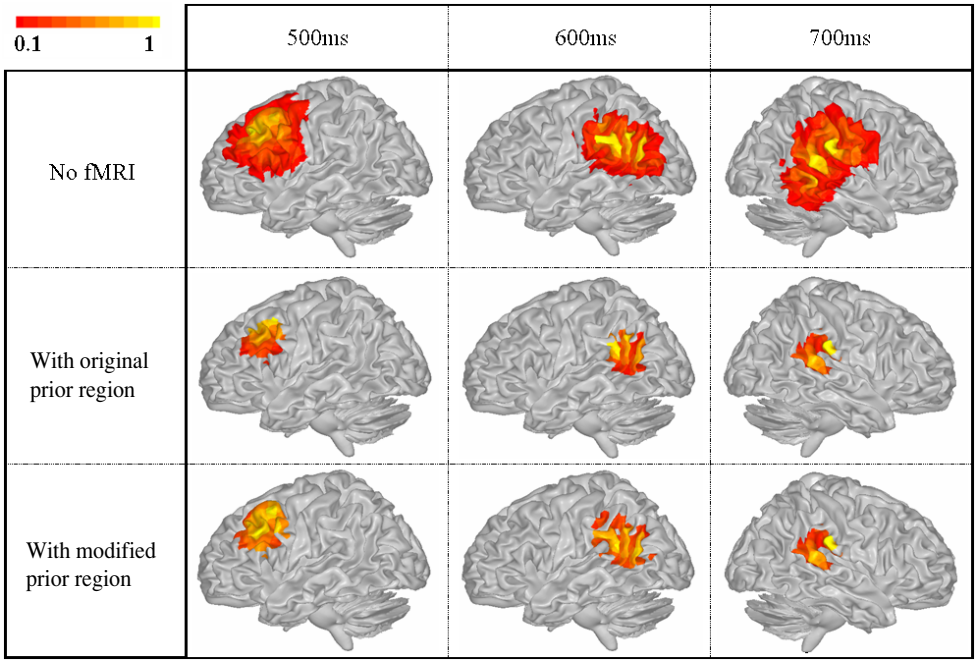

Figure 8. Normalized current dipole power at 500 ms, 600 ms and 700 ms, estimated for case 1 under three different conditions (no fMRI information, with original prior activation regions and with modified prior activation regions). Sources that exceed 0.1 are visualized. SNR = 7 dB.

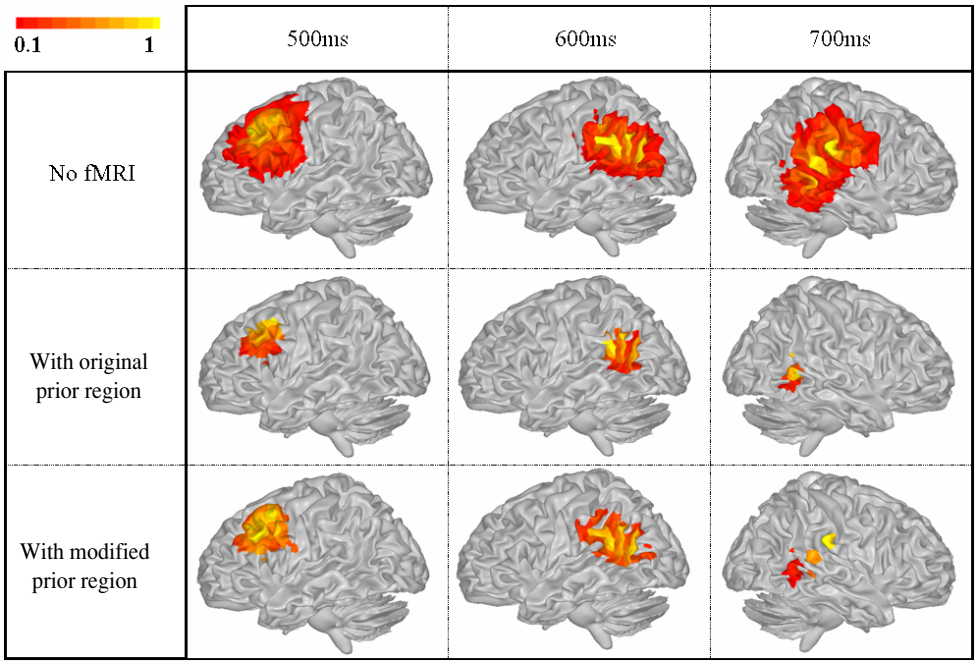

Figure 9. Normalized current dipole power at 500 ms, 600 ms and 700 ms, estimated for case 2 under three different conditions (no fMRI information, with original prior activation regions and with modified prior activation regions). Sources that exceed 0.1 are visualized. SNR = 7 dB.

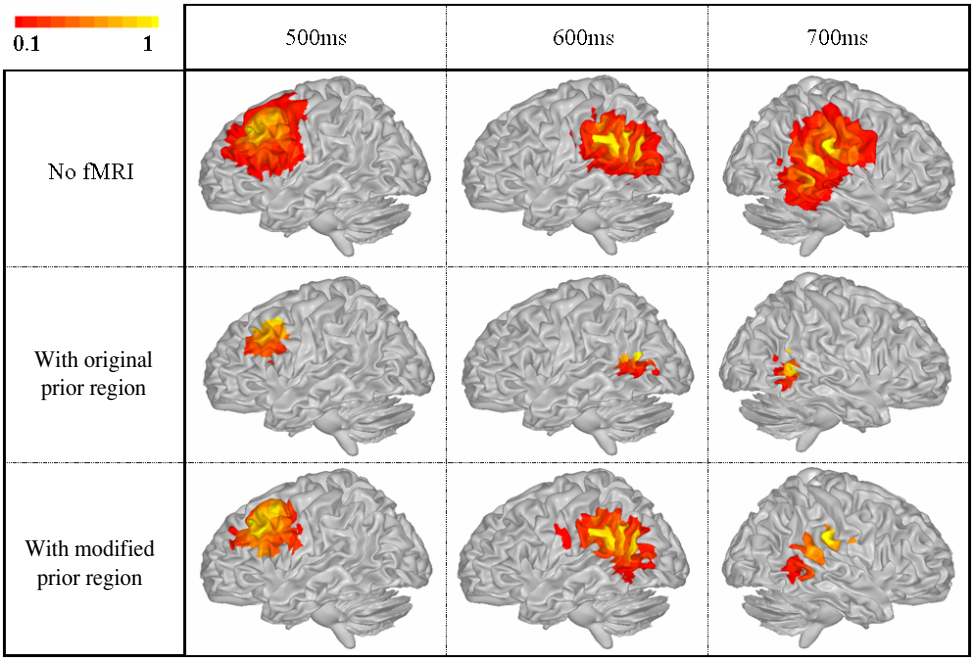

Figure 10. Normalized current dipole power at 500 ms, 600 ms and 700 ms, estimated for case 3 under three different conditions (no fMRI information, with original prior activation regions and with modified prior activation regions). Sources that exceed 0.1 are visualized. SNR = 7 dB.

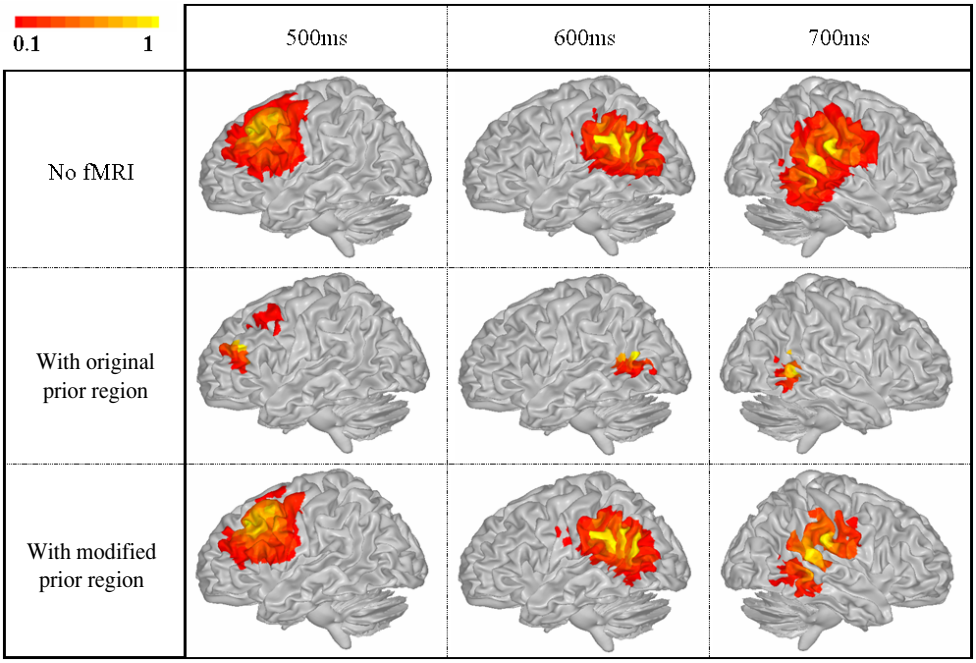

Figure 11. Normalized current dipole power at 500 ms, 600 ms and 700 ms, estimated for case 4 under three different conditions (no fMRI information, with original prior activation regions and with modified prior activation regions). Sources that exceed 0.1 are visualized. SNR = 7 dB.

In summary, the proposed technique can be an alternative tool which enables us to selectively apply fMRI prior information to EEG/MEG source imaging. When there is no significant mismatch between fMRI and EEG/MEG sources, the use of the proposed technique rarely influences the advantage of the fMRI-constrained EEG/MEG source imaging. When there are significant mismatches between the two different modalities, however, the proposed technique weakens the influence of the fMRI constraint by modifying the prior activation regions by compulsion, resulting in widespread but more reasonable source estimates representing the actual EEG/MEG source locations correctly.

4. Conclusions

The present preliminary simulation study demonstrated that significant mismatches between fMRI and EEG/MEG sources, which may cause misidentification of neuronal source locations, can possibly be considered in the fMRI-constrained EEG/MEG source imaging approaches. The proposed technique extended the prior activation regions by including significant EEG/MEG sources, of which the adjacent areas were identified by partial time integration of conventional source imaging results without *a priori* information, into the modified prior activation regions. Such a strategy allowed users to 'selectively' apply the fMRI constraint to the EEG/MEG source imaging. In other words, hard fMRI constraint is applied only when there is no significant mismatch between the two modalities; while weakened fMRI constraint is applied when there exist significant mismatches.

Although this preliminary simulation study has suggested an alternative approach to consider the fMRI mismatch sources in EEG/MEG source imaging and showed a good example of its possible applications, the present study may have some limitations. One fundamental assumption of the proposed technique was that all the true source locations are revealed in the unconstrained solution. Although we applied partially integrated source intensity not to ignore EEG/MEG sources with short durations, it is still possible that some EEG/MEG sources with relatively small intensities might not be reflected in the partially integrated source image, which may result in missing activations at some time slices.

We have used partially integrated source intensity to estimate possibly significant source activity. Typically, however, significance has been assessed using a statistic computed from intensity such as the dynamic statistical parametric map (dSPM) (Dale *et al* 2000). It has been reported that the effect of using fMRI weightings rather than unconstrained minimum norm is much less in the dSPM than in the current density maps, since in addition to increasing source strength in those areas where fMRI activity occurs these methods also increase noise variance in these same locations. The use of statistical approaches to estimate possibly significant source activity and comparison between the two methods will be performed in the future study.

Contrary to the conventional fMRI-constrained EEG/MEG source imaging approaches (Ahlfors and Simpson 2004, Liu *et al* 2006), the proposed technique is neither linear nor straightforward since it requires an additional step to calculate partial integration of source intensities at all time slices, resulting in increased computational cost and difficulties in data analysis. Nevertheless, since the linear inverse operator in (1) was unchanged for the whole time window after saving it in computer memory, the computational time could be considerably saved.

In the present study, we have assumed four different cases according to the mismatch levels between true source locations and fMRI activation regions. In future studies, we will additionally perform different case studies such as artificial fMRI-extended sources and fMRI

invisible sources. The efficiency and usefulness of the proposed technique will be verified more robustly by Monte Carlo simulation studies and *in vivo* data analysis.

Acknowledgments

This work was supported in part by a grant of the Korea Health 21 R&D Project, Ministry of Health and Welfare, Korea (02-PJ3-PG6-EV07-0002), and in part by a grant (M103KV010016-06K2201-01610) from Brain Research Center of the 21st Century Frontier Research Program funded by the Ministry of Science and Technology of the Republic of Korea.

References

Ahlfors S P *et al* 1999 Spatiotemporal activity of a cortical network for processing visual motion revealed by MEG and fMRI *J. Neurophysiol.* **82** 2545–55

Ahlfors S P and Simpson G V 2004 Geometrical interpretation of fMRI-guided MEG/EEG inverse estimates *Neuroimage* **22** 323–32

Babiloni F, Babiloni C, Carducci F, Romani G L, Rossini P M, Angelone L M and Cincotti F 2003 Multimodal integration of high-resolution EEG and functional magnetic resonance imaging data: a simulation study *Neuroimage* **19** 1–15

Babiloni F, Mattia D, Babiloni C, Astolfi L, Salinari S, Basilisco A, Rossini P M, Marciani M G and Cincotti F 2004 Multimodal integration of EEG, MEG and fMRI data for the solution of the neuroimage puzzle *Magn. Res. Image.* **22** 1471–6

Baillet S, Riera J J, Marin G, Mangin J F, Aubert J and Garnero L 2001 Evaluation of inverse methods and head models for EEG source localization using a human skull phantom *Phys. Med. Biol.* **46** 77–96

Bonmassar G, Schwartz D P, Liu A K, Kwong K K, Dale A M and Belliveau J W 2001 Spatiotemporal brain imaging of visual-evoked activity using interleaved EEG and fMRI recordings *Neuroimage* **13** 1035–43

Dale A M, Fischl B and Sereno M I 1999 Cortical surface-based analysis: I. Segmentation and surface reconstruction *Neuroimage* **9** 179–94

Dale A M, Liu A K, Fischl B R, Buckner R L, Belliveau J W, Lewine J D and Halgren E 2000 Dynamic statistical parametric mapping: combining fMRI and MEG for high-resolution imaging of cortical activity *Neuron* **26** 55–67

Dale A M and Sereno M I 1993 Improved localization of cortical activity by combining EEG and MEG with MRI surface reconstruction: a linear approach *J. Cognit. Neurosci.* **5** 162–76

Disbrow E A, Slutsky D A, Roberts T P L and Krubitzer L A 2005 Functional MRI at 1.5 tesla: a comparison of the blood oxygenation level-dependent signal and electrophysiology *Proc. Natl. Acad. Sci. USA* **97** 9718–23

Dhond R P, Marinkovic K, Dale A M, Witzel T and Halgren E 2003 Spatiotemporal maps of past-tense verb inflection *Neuroimage* **19** 91–100

Fischl B and Dale A M 2000 Measuring the thickness of the human cerebral cortex from magnetic resonance images *Proc. Natl. Acad. Sci. USA* **97** 11050–5

Fujimaki N, Hayakawa T, Nielsen M, Knösche T R and Miyauchi S 2002 An fMRI-constrained MEG source analysis with procedures for dividing and grouping activation *Neuroimage* **17** 324–43

George J S, Aine C J, Mosher J C, Schmidt D M, Ranken D M, Schlitt H A, Wood C C, Lewine J D, Sanders J A and Belliveau J W 1995 Mapping function in the human brain with magnetoencephlaography, anatomical magnetic-resonance-imaging, and functional magnetic-resonance-imaging *J. Clin. Neurophysiol.* **12** 406–31

Gonzalez Andino S L, Blanke O, Lantz G, Thut G and Grave de Peralta Menendez R 2001 The use of functional constraints for the neuroelectromagnetic inverse problem: alternatives and caveats *Int. J. Bioelectrom.* **3** (1) (www.ijbem.org)

Gorodnistky I F, George J S and Rao B D 1995 Neuromagnetic imaging with FOCUSS: a recursive weighted minimum norm algorithm *Electroenceph. Clin. Neurophys.* **95** 231–51

Hämäläinen M S and Sarvas J 1989 Realistic conductivity geometry model of the human head for interpretation of neuromagnetic data *IEEE Trans. Biomed. Eng.* **36** 165–71

Hansen P 1992 Analysis of discrete ill-posed problems by means of the L-curve *SIAM Rev.* **34** 561–80

Haueisen J, Ramon C, Eiselt M, Brauer H and Nowak H 1997 Influence of tissue resistivities on neuromagnetic fields and electric potentials studied with a finite element model of the head *IEEE Trans. Biomed. Eng.* **44** 727–35

He B, Musha T, Okamoto Y, Homma S, Nakajima Y and Sato T 1987 Electric dipole tracing in the brain by means of the boundary element method and its accuracy *IEEE Trans. Biomed. Eng.* **34** 406–14

Im C H, An K O, Jung H K, Kwon H and Lee Y H 2003 Assessment criteria for MEG/EEG cortical patch tests *Phys. Med. Biol.* **48** 2561–73

Im C H, Jung H K and Fujimaki N 2005 fMRI-constrained MEG source imaging and consideration of fMRI invisible sources *Hum. Brain Mapp.* **26** 110–8

Kincses W E, Braun C, Kaiser S and Elbert T 1999 Modeling extended sources of event-related potentials using anatomical and physiological constraints *Hum. Brain Mapp.* **8** 182–93

Korvenoja A, Aronen H J and Ilmoniemi J 2001 Functional MRI as a constraint in multi-dipole models of MEG data *Int. J. Bioelectrom.* **3** (1) (www.ijbem.org)

Korvenoja A, Huttunen J, Salli E, Pohjonen H, Martinkauppi S, Palva J M, Lauronen L, Virtanen J, Ilmoniemi R J and Aronen H J 1999 Activation of multiple cortical areas in response to somatosensory stimulation: combined magnetoencephalographic and functional magnetic resonance imaging *Hum. Brain Mapp.* **8** 13–27

Lin F H, Witzel T, Hämäläinen M S, Dale A M, Belliveau J W and Stufflebeam S M 2004 Spectral spatiotemporal imaging of cortical oscillations and interactions in the human brain *Neuroimage* **23** 582–95

Liu A K, Belliveau J W and Dale A M 1998 Spatiotemporal imaging of human brain activity using functional MRI constrained magnetoencephalography data: Monte Carlo simulations *Proc. Natl. Acad. Sci. USA* **95** 8945–50

Liu A K, Dale A M and Belliveau J W 2002 Monte Carlo simulation studies of EEG and MEG localization accuracy *Hum. Brain Mapp.* **16** 47–62

Liu Z, Ding L and He B 2006 Integration of EEG/MEG with MRI and fMRI—high-resolution, multimodal neuroimaging *IEEE Eng. Med. Biol. Mag.* **25** 46–53

Nunez P L and Silberstein R B 2000 On the relationship of synaptic activity to macroscopic measurements: does co-registration of EEG with fMRI make sense? *Brain Topogr.* **13** 79–96

Nunez P L and Srinivasan R 2005 *Electric Fields of the Brain : The Neurophysics of EEG* 2nd edn (Oxford: Oxford University Press)

Oostendorp T F, Delbeke J and Stegeman D F 2000 The conductivity of the human skull: results of *in vivo* and *in vitro* measurements *IEEE Trans. Biomed. Eng.* **47** 1487–92

Opitz B, Mecklinger A, von Cramon D Y and Kruggel F 1999 Combining electrophysiological and hemodynamic measures of the auditory oddball *Psychophysiology* **36** 142–7

Pascual-Marqui R D, Michel C M and Lehmann D 1994 Low resolution electromagnetic tomography: a new method for localizing electrical activity in the brain *Int. J. Psychophysiol.* **18** 49–65

Phillips C, Mattout J, Rugg M D, Maquet P and Friston K J 2005 An empirical Baysian solution to the source reconstruction problem in EEG *Neuroimage* **24** 997–1011

Rothman D L, Sibson N R, Hyder F, Shen J, Behar K L and Shulman R G 1999 *In vivo* MRS studies of the relationship between glutamine–glutamine neurotransmitter cycle and functional neuroenergetics *Phil. Trans. R. Soc.* B **354** 1165–7

Sato M-a, Yoshioka T, Kajihara S, Toyana K, Goda N, Doya K and Kawato M 2004 Hierarchical Bayesian estimation for MEG inverse problem *Neuroimage* **23** 806–26

Sekihara K, Nagarajan S S, Poeppel D, Marantz A and Miyashita Y 2001 Reconstructing spatio-temporal activities of neural sources using an MEG vector beamformer technique *IEEE Trans. Biomed. Eng.* **48** 760–71

Shattuck D W and Leahy R M 2002 BrainSuite: An automated cortical surface identification tool *Med. Image Anal.* **6** 129–42

Torquati K, Pizzella V, Babiloni C, Gratta C D, Penna S D, Ferretti A, Franciotti R, Rossini P M and Romani G L 2005 Nociceptive and non-nociceptive sub-regions in the human secondary somatosensory cortex: an MEG study using fMRI constraints *Neuroimage* **26** 48–56

Vanni S, Warnking J, Dojat M, Delon-Martin C, Bullier J and Segebarth C 2004 Sequence of pattern onset responses in the human visual areas: an fMRI constrained VEP source analysis *Neuroimage* **21** 801–17

Vitacco D, Brandeis D, Pascual-Marqui R and Martin E 2002 Correspondence of event-related potential tomography and functional magnetic resonance imaging during language processing *Hum. Brain Mapp.* **17** 4–12

Wagner M and Fuchs M 2001 Integration of functional MRI, structural MRI, EEG and MEG *Int. J. Bioelectron.* **3** (1) (www.ijbem.org)

Wagner M, Fuchs M and Kastner J 2000 fMRI-constrained dipole fits and current density reconstructions *Proc. Biomag2000*